Acta Crystallographica Section B
Structural Science
ISSN 0108-7681

Solvothermal synthesis, multi-temperature crystal structures and physical properties of isostructural coordination polymers, $2C_4H_{12}N^+$-$[M_3(C_8H_4O_4)_4]^{2-}\cdot 3C_5H_{11}NO$, M = Co, Zn

Rasmus Damgaard Poulsen, Anders Bentien, Mogens Christensen and Bo Brummerstedt Iversen*

Department of Chemistry, University of Aarhus, DK-8000 Aarhus C, Denmark

Correspondence e-mail: bo@chem.au.dk

Received 21 September 2005
Accepted 22 December 2005

Two isostructural metal organic framework (MOF) structures have been synthesized by solvothermal methods and examined by single-crystal X-ray diffraction. A microcrystal of $2C_4H_{12}N^+[Co_3(C_8H_4O_4)_4]^{2-}\cdot 3C_5H_{11}NO$ (1) was investigated at T = 120 K using synchrotron radiation. $2C_4H_{12}N^+$-$[Zn_3(C_8H_4O_4)_4]^{2-}\cdot 3C_5H_{11}NO$ (2) was investigated at multiple temperatures (T = 30, 100, 200 and 300 K) on a conventional diffractometer. The thermal expansion of the structure of (2) is anisotropic and along the a axis, which corresponds to the metal chain direction. The structures contain anionic frameworks with cations and solvent molecules trapped in the voids. The magnetic susceptibility (χ) and heat capacity (C_p) have been measured from 1.8 to 350 K. Compound (1) orders ferromagnetically with a broad phase transition observed in C_p at $\sim$ 6 K. The magnetic moment reaches a value of 3 μ_B per Co at 2 K in a magnetic field of 9 T, and a Curie–Weiss fit to $\chi(T)$ gives an effective moment (μ_{eff}) of 4.2 μ_B and a Weiss temperature (θ) of 23 K. The exchange mechanism for the magnetic coupling is suggested to involve the Co—O—Co bridges in the individual three-metal-atom subchains. The three-dimensional magnetism presumably is due to superexchange through two out of the three unique $C_8H_4O_4$ linker molecules, which have the carboxylate and benzene π systems well aligned.

1. Introduction

The synthesis and characterization of new coordination polymers, also called metal organic frameworks (MOFs), have spurred enormous interest (Li *et al.*, 1999; Chen *et al.*, 2001; Noro *et al.*, 2002; Lu, 2003; Yaghi *et al.*, 2003; Kitahawa *et al.*, 2004). The attractive feature of MOFs, compared, for example, with zeolites, is that the basic molecular building blocks (reactants) are preserved in the final assembled network. This feature offers the possibility of designing networks in which both pore size and physical/chemical properties are manipulated when the basic components are changed. Numerous coordination polymers have been synthesized with an amazing variety of one-, two- and three-dimensional structural characteristics (Sudik *et al.*, 2005). One driving force for studying MOFs is the potential application for gas storage in the open volume in the nanoporous voids (Eddaoudi *et al.*, 2000, 2002; Rosi *et al.*, 2003; Chae *et al.*, 2004; Rowsell *et al.*, 2005). Other studies have explored the quantum confinement effects on molecules trapped in nanopores (Kobayashi *et al.*, 2003). One of the initial interests in coordination polymers was to study

magnetic properties (Miller & Epstein, 1995; Price *et al.*, 2001). The 'Lego®' molecular building block approach in these systems may provide novel systems for fundamental studies of magnetic exchange mechanisms. Since the organic linker molecule can be incrementally increased in length as well as designed with specific electronic properties, it may be possible to fine-tune the magnetic interaction pathways between the metal centers. The study of magnetic MOFs is strengthened if one can fabricate isostructural non-magnetic frameworks (Tynan *et al.*, 2004). However, these can be difficult to obtain because the coordination properties of the different transition metals have significant variation.

In the present paper we report on the synthesis, crystal structures and physical properties of two new nanoporous coordination polymers, $2C_4H_{12}N^+[Co_3(C_8H_4O_4)_4]^{2-}\cdot 3C_5H_{11}NO$ (1) and $2C_4H_{12}N^+[Zn_3(C_8H_4O_4)_4]^{2-}\cdot 3C_{15}H_{11}NO$ (2), which are isostructural and have complementary magnetic properties. The structures of (1) and (2) consist of chains of metal atoms interconnected by benzene-1,4-dicarboxylate (BDC) linkers giving a three-dimensional network. The framework has a layer-like structure with open pores between the layers, while the layers themselves are somewhat blocked in the third dimension as a result of cross-linking by the BDC moiety. Contrary to many other MOFs the frameworks of (1) and (2) are anionic (Rosi *et al.*, 2002) and they are stabilized by $NH_2(C_2H_5)_2^+$ solvent cations (Chen *et al.*, 2003). The *N*,*N*-diethylformamide (DEF) solvent molecules are located in the cavities and, because there are multiple hydrogen bonds to either the framework or the diethylammonium (DEA) cations, the DEF solvent molecules have well defined positions at low temperature. For the ferromagnetic compound (1) the structure was challenging to obtain because of severe twinning of the crystals. Only after an extensive search was it possible to obtain single-crystal data on a minute crystal at a third-generation synchrotron source. We have previously used synchrotron radiation to study magnetic MOFs, where the coupling of microscopic electronic structure information obtained from X-ray charge-density analysis and macroscopic magnetic measurements led to a detailed account of the physical properties (Poulsen *et al.*, 2004, 2005). Owing to the weakness of the diffraction from our crystals of (1) this has not been possible in the present case. On the other hand, we have an isostructural nonmagnetic reference structure available in the present study, and multi-temperature single-crystal X-ray diffraction data on (2) (including helium cryocooling) reveal important structural rearrangements, which presumably are required in (1) for the magnetic ordering to occur.

2. Experimental

2.1. Synthesis

The syntheses of (1) and (2) are one pot reactions. For (1) a mixture of 1,4-benzene dicarboxylic acid (H_2BDC, 0.166 g, 1 mmol) and DEF (8 ml) was added to $Co(NO_3)_2\cdot 6H_2O$ (0.294 g, 1 mmol) dissolved in DEF (2 ml). The mixture was kept at 375 K for 72 h in a 12 ml autoclave. The crystals formed were rhombic in shape and purple. For (2) a mixture of H_2BDC (0.166 g, 1 mmol) and DEF (4 ml) was added to $Zn(NO_3)_2\cdot 6H_2O$ (0.298 g, 1 mmol) dissolved in DEF (2 ml). The mixture was kept at 375 K for 72 h in an autoclave. The crystals formed were rhombic in shape and transparent white. The crystals of (2) are mechanically robust, whereas those of (1) are fragile and tend to split into layers.

2.2. Physical properties

The total heat capacities (C_p) of (1) and (2), and the magnetic susceptibility (χ) of (1), were measured from 2 to 350 K on a Quantum Design Physical Properties Measurement System (PPMS) at the Department of Chemistry, University of Aarhus, using pellets pressed from finely ground powder. Thermogravimetric analysis (TGA) and differential thermal analysis (DTA) were carried out from 298 to 973 K using a Stanton–Redcroft TGA–DTA simultaneous thermal analyzer STA 1000/1500. A heating rate of 10 K min^{-1} was applied in an Ar gas flow. To examine the purity of the bulk samples, X-ray powder diffraction data were measured on a Stoe diffractometer at the Department of Chemistry, University of Aarhus, using Cu $K\alpha_1$ radiation from a Ge(111) monochromator and a position-sensitive detector covering 40° in 2θ.

2.3. X-ray data collection

A purple crystal of (1) (0.040 × 0.060 × 0.090 mm^3) was mounted in oil on a glass fiber. Testing of more than 20 crystal specimens was carried out at the synchrotron before a single crystal was found. The crystals have very prominent twinning owing to the layering of flat plates. The sample was mounted on a six-circle Kuma diffractometer at the Swiss–Norwegian Beamline at ESRF, Grenoble, equipped with an Oxford CCD detector system. The data collection was carried out at a wavelength of 0.710 Å obtained from a double Si(111) crystal monochromator. The temperature was kept at 120 K using an Oxford nitrogen Cryostream. The ω- and φ-scan experiment used a step width of 0.3°. In total 180 772 reflections were integrated with *CrysAlis RED* (Oxford Diffraction, 2004), whereas an empirical absorption correction was performed with the *SADABS* program (Sheldrick, 2003).

For (2) a transparent white crystal (0.250 × 0.250 × 0.300 mm^3) was mounted in protective oil on a glass fiber glued to a small copper wire. This was mounted on a brass pin, which was placed on the goniometer of a SMART 1K diffractometer at the Department of Chemistry, University of Aarhus. The experiment was carried out at 300, 200 and 100 K, and subambient conditions were achieved with a cold N_2 stream of an Oxford Cryostream device. The ω- and φ-scan experiment used a step width of 0.3°. In total 50 934 reflections at 300 K, 66 955 reflections at 200 K and 67 722 reflections at 100 K were integrated with *SAINT-Plus* (Sheldrick, 2003). Empirical absorption corrections were made with the *SADABS* program (Sheldrick, 2003). Data at 30 K were measured on (2) at the Department of Chemistry, University of Durham, UK. A plate-shaped crystal (0.250 × 0.270 × 0.050 mm^3) was mounted on a brass pin, which was placed on

Table 1
Crystallographic data.

The second entry in the first column shows the residual for a data cut-off at sin θ/λ = 0. Å^{-1}.

Sample	(1)	(2)	(2)	(2)	(2)
T (K)	120	30	100	200	300
Formula	$Co_3O_{19}N_5C_{55}H_{73}$	$Zn_3O_{19}N_5C_{55}H_{73}$	$Zn_3O_{19}N_5C_{55}H_{73}$	$Zn_3O_{19}N_5C_{55}H_{73}$	$Zn_3O_{19}N_5C_{55}H_{73}$
Formula weight (g mol^{-1})	1284.98	1304.30	1304.30	1304.30	1304.30
Space group	*C*2/*c*	*C*2/*c*	*C*2/*c*	*C*2/*c*	*C*2/*c*
Sample size (µm)	40 × 60 × 90	250 × 270 × 50	250 × 250 × 300	250 × 250 × 300	250 × 250 × 300
a (Å)	33.3112 (7)	33.2613 (5)	33.3307 (5)	33.4193 (4)	33.5639 (5)
b (Å)	9.8336 (3)	9.7844 (1)	9.8105 (1)	9.8455 (1)	9.8791 (2)
c (Å)	18.2963 (5)	18.2156 (3)	18.1988 (3)	18.1908 (2)	18.1814 (3)
β (°)	92.354 (2)	92.613 (1)	92.552 (1)	92.495 (1)	92.350 (1)
V (Å^3)	5988.24 (20)	5921.95 (10)	5944.94 (16)	5979.64 (14)	6023.54 (17)
ρ (g cm^{-3})	1.425	1.463	1.457	1.449	1.438
λ (Å)	0.710	0.7107	0.7107	0.7107	0.7107
μ (mm^{-1})	1.425	1.27	1.27	1.27	1.27
N_{meas}, N_{unique}	180 772, 24 905	27 952, 9377	67 722, 9010	66 955, 8640	50 934, 5311
R_{int}	0.089	0.0912	0.1044	0.1105	0.0891
sin θ/λ (Å^{-1})	1.09 0.7	0.74	0.72	0.70	0.59
N_{obs}, N_{var}	24 905, 430† 8282, 430†	9377, 430†	9010, 430†	8640, 412†	5311, 412†
$R(F)_{2\sigma}$ (N_F)	0.0809 (15 944) 0.0600 (6866)	0.0404 (7243)	0.0605 (5722)	0.0536 (5093)	0.0400 (3677)
$R(F)_{all}$ (N_F)	0.1460 (24 905) 0.0829 (8282)	0.0543 (9377)	0.1243 (9010)	0.1242 (8640)	0.0805 (5311)
$R_w(F^2)_{all}$ (N_F)	0.1990 (24 905) 0.1514 (8282)	0.0858 (9377)	0.1173 (9010)	0.1173 (8640)	0.1027 (5311)
S_{all} (N_F)	1.245 (24 905) 1.097 (8282)	0.960 (9377)	1.026 (9010)	0.993 (8640)	1.000 (5311)

† The change in the number of parameters from 430 to 412 is due to the constraint of equal anisotropic displacement parameters in the disordered C32*A*/C33*A* and C32*B*/C33*B* ethyl groups.

the goniometer of a Bruker APEX diffractometer. The cooling was performed with an Oxford Cryosystem HELIX. The ω-scan experiment used a step width of 0.3°, and a total of 27 352 reflections were integrated with *SAINT* (Sheldrick, 2003). A face-indexed absorption correction was carried out in the program *XPREP* (Sheldrick, 2003). The structures of (1) and (2) were solved using the direct methods program *SHELX* (Sheldrick, 2003). All H atoms bound to C atoms

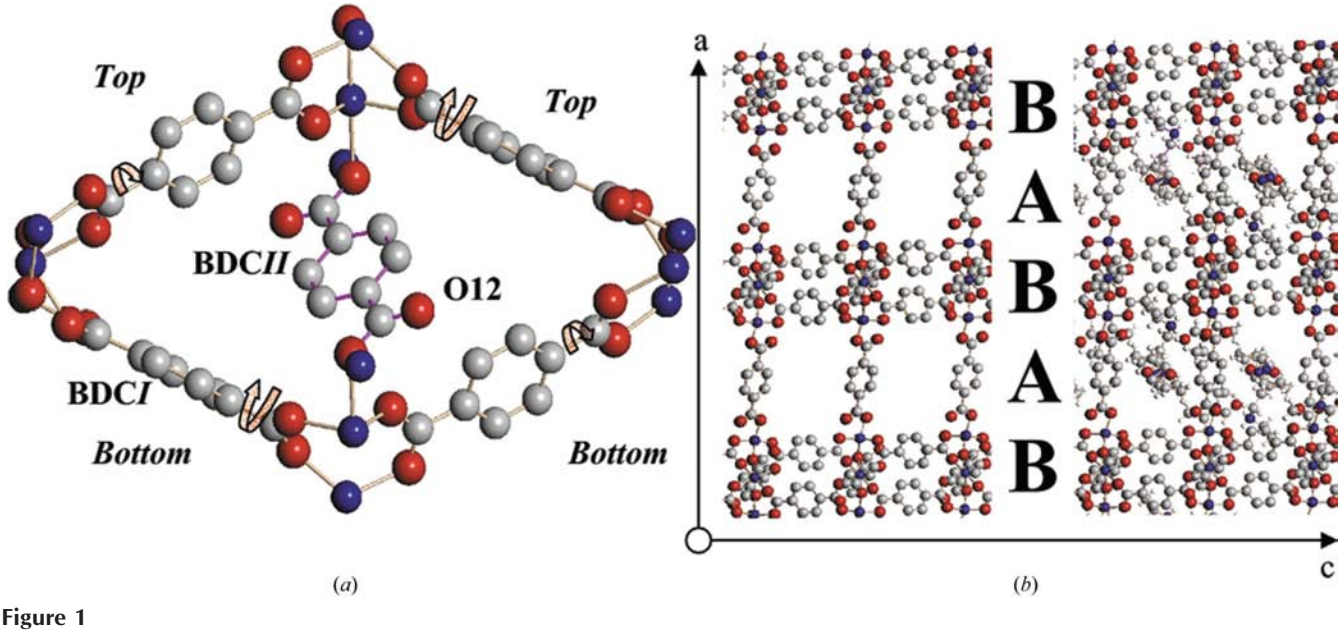

Figure 1
(*a*) The rhombic void in the *B* layer spanned by the *BDCI* linker and the diagonal stabilizing *BDCII* linker. Curly arrows show the large twist of ∼17–18° of the O28/C28/O29 carboxylate group of *BDCI*. The terminal O12 atom of the *BDCII* linker is clearly seen. (*b*) The framework channels viewed along the *b* axis. In the channels to the right solvent molecules have been included.

Table 2
Selected torsion angles (°) of the carboxylate groups.

	(1): 120 K	(2): 30 K	(2): 100 K	(2): 200 K	(2): 300 K
O1—C1—C2—C3	4.4 (3)	6.1 (3)	4.7 (3)	4.6 (3)	6.6 (3)
O2—C1—C2—C3	5.3 (5)	6.6 (2)	6.3 (4)	6.2 (5)	7.6 (6)
O11—C11—C12—C13	0.5 (3)	0.2 (2)	0.2 (3)	1.0 (3)	2.3 (3)
O12—C11—C12—C13	3.2 (5)	2.9 (3)	3.6 (4)	3.9 (4)	5.0 (5)
O21—C21—C22—C23	3.0 (5)	4.2 (3)	4.1 (4)	3.9 (4)	3.4 (5)
O22—C21—C22—C23	5.4 (3)	4.3 (3)	5.0 (3)	5.3 (3)	5.6 (3)
O28—C28—C25—C26	18.2 (3)	17.2 (2)	17.8 (3)	18.2 (3)	18.6 (4)
O29—C28—C25—C26	17.1 (4)	17.1 (3)	17.2 (4)	18.1 (4)	18.3 (5)

were placed in calculated positions and allowed to ride during subsequent refinement. Further experimental details are listed in Table 1.

3. Results and discussion

3.1. The framework

The isostructures of (1) and (2) consist of chains of metal atoms interconnected by the BDC linkers forming a three-dimensional layer-like network with large cavities (Figs. 1 and 2). There are three structurally unique BDC linkers and these are in the following named *BDCI*, *BDCII* and *BDCIII*. The metal chains can be subdivided into small chains of three metals bridged by the *BDCIII* linker molecule, and the result is an *ABAB* layered structure (Fig. 1*b*). The metal atom subchains are interconnected *via BDCI* and *BDCII* to give a rhombic void in the *B* layer with the length of the short diagonal corresponding to the approximate length of a BDC molecule. Fig. 1(*a*) shows how *BDCI* bridges the metal atoms with direct bonding between the carboxylate groups and the four metal atom subchains. The four corners of the rhombic void are interconnected *via* a '*top–top–bottom–bottom*' bonding mode, where *top* corresponds to the two metal atoms at the top of the three metal atom subchain and *bottom* to the two metals at the bottom. The unit is stabilized by *top-to-bottom* diagonal bonding of *BDCII*, shown as purple bonds in Fig. 1(*a*). Atom O11 of the O11/C11/O12 carboxylate group of *BDCII* bridges two metal atoms of the metal subchain, while atom O12 has no bonding to the metal atoms. Thus, O12 is a terminal atom with respect to the framework. The cross-link stabilization of *BDCII* results in a lack of space for solvent inclusion in the *B* layer. The porous framework is formed when the *BDCIII* linkers join the *B* layers and form large cavities for solvent storage in the *A* layer (Fig. 1*b*). Indeed, solvent is present in the *A* layer, and the asymmetric unit contains 1.5 DEF molecules, *DEFI* and *DEFII*, and one diethylammonium cation, *DEA*, in the void (Fig. 1*b*).

The structural unit of the *B* layer has been observed previously for three other Zn-based MOFs. Chen *et al.* (2003) prepared a three-dimensional anionic framework with mixed carboxylate linkers. The structure consists of subchains of three Zn atoms with the same tetrahedral and octahedral coordination as in (1) and (2). However, since the interconnection is achieved with a very different linker, benzene-1,3,5-tricarboxylic acid, the subchains are neither parallel nor in layers. Like (1) and (2) the structure of Chen *et al.* (2003) is anionic with free terminal carboxylate O atoms stabilized by $NH_2(CH_3)_2^+$ cations. Edgar *et al.* (2001) have prepared a two-dimensional layered MOF system based on Zn^{2+} metal ions, BDC linkers and DMF solvent molecules. This structure has the same features as the *B* layer in (1) and (2), *i.e.* subchains of three metal atoms with tetrahedral and octahedral coordination, and a diagonal linker with a terminal unbound O atom. The main difference with respect to (1) and (2) is the lack of interconnection between the Zn subchains in adjacent layers. In the structure of Edgar *et al.* (2001) a water molecule bonds axially to Zn1 and thereby terminates the chains. The DMF solvent molecules are located in the voids with no direct bonding to the *B* layer. The subchains in the individual layers are parallel but not aligned in three dimensions. Furthermore, since the DMF and water molecules are smaller than the DEF solvent molecules of (1) and (2), the former can fit into the small cavities of the *B* layer. In the Edgar *et al.* (2001) structure the packing of the layers originates from hydrogen bonds between the terminal water molecule and a DMF molecule of the adjacent layer. Contrary to the structures of (1) and (2) the structure is not stable and it transforms into a new MOF structure with time. Structurally unstable Zn–BDC–DMF-based MOFs have also been reported by Clausen *et al.* (2005), where a kinetic MOF product obtained directly from solvothermal synthesis slowly rearranged into a thermodynamically stable MOF structure. An alternative MOF system based on Zn^{2+} and BDC linkers with methanol as the solvent was prepared by Li *et al.* (1998). This structure is not layered but again contains subchains consisting of three Zn atoms, which show coordination features similar to the metal subchains in the *B* layers of (1) and (2). The main difference is the interconnection of the Zn subchains. In the structure of Li *et al.* (1998) two methanol molecules bond directly to *M*1, thus terminating the chains. Additionally, a single MeOH solvent molecule is located in the cavity. As in (1) and (2), the diagonal BDC linker has a terminal unbound O atom. The linker bonds from the two top Zn atoms of one subchain to the two bottom Zn atoms of an adjacent subchain parallel to the first subchain, thus creating a chain of subchains aligned parallel to each other. However, the BDC linker analogous to the BDCI linkers of (1) and (2) do not form a rhombic void. Instead the BDC linker bonds from the two top Zn atoms of one Zn subchain to the bottom of an out-of-plane subchain parallel to the first. This connectivity creates a three-dimensional framework with bound and unbound MeOH solvent molecules located in the cavities of the structure.

The molecular self-assemblies of (1) and (2) are carried out under solvothermal conditions, and whether the negatively charged framework is a result of the formation of cations from isolated solvent reactions or the opposite is an open question. We have used DEF as the solvent in other solvothermal reactions with different metal ions and linkers, and here the formation and inclusion of cations in the MOFs have not been observed (Poulsen *et al.*, 2005). Hence, the driving force for the formation of solvent cations may be the specific configuration of the assembled framework. The solvothermal

Table 3
Selected bond lengths (Å) of (1) and (2).

	(1): 120 K	(2): 30 K	(2): 100 K	(2): 200 K	(2): 300 K
*M*1—*M*2	3.239 (3)	3.247 (1)	3.255 (2)	3.269 (2)	3.288 (2)
*M*1—O1	1.940 (3)	1.926 (1)	1.928 (2)	1.926 (2)	1.925 (2)
*M*1—O11	1.998 (2)	1.979 (1)	1.987 (2)	1.985 (2)	1.995 (2)
*M*1—O21	1.982 (2)	1.966 (1)	1.966 2)	1.969 (2)	1.970 (2)
*M*1—O28	1.979 (2)	1.978 (1)	1.979 (2)	1.981 (2)	1.982 (2)
*M*2—O11	2.217 (2)	2.220 (1)	2.234 (2)	2.250 (2)	2.277 (2)
*M*2—O22	2.053 (2)	2.051 (1)	2.053 (2)	2.049 (2)	2.045 (2)
*M*2—O29	2.040 (2)	2.019 (1)	2.025 (2)	2.026 (2)	2.028 (2)
O1—C1	1.295 (4)	1.290 (2)	1.291 (3)	1.288 (4)	1.279 (4)
O2—C1	1.236 (4)	1.234 (2)	1.232 (3)	1.231 (4)	1.223 (4)
O11—C11	1.307 (4)	1.306 (2)	1.299 (3)	1.302 (3)	1.296 (4)
O12—C11	1.243 (4)	1.232 (2)	1.238 (3)	1.238 (3)	1.234 (4)
O21—C21	1.277 (4)	1.275 (2)	1.275 (3)	1.263 (4)	1.264 (4)
O22—C21	1.259 (4)	1.256 (2)	1.248 (3)	1.256 (3)	1.251 (4)
O28—C28	1.270 (4)	1.267 (2)	1.264 (3)	1.264 (3)	1.261 (4)
O29—C28	1.260 (4)	1.260 (2)	1.253 (3)	1.249 (3)	1.244 (4)

Table 4
Bond angles (°) of the two metal atoms in (1) and (2).

	(1): 120 K	(2): 30 K	(2): 100 K	(2): 200 K	(2): 300 K
O1—*M*1—O11	128.8 (1)	127.89 (5)	128.43 (9)	129.77 (9)	130.4 (1)
O1—*M*1—O21	112.6 (1)	114.54 (5)	114.11 (8)	113.60 (9)	112.7 (1)
O1—*M*1—O28	93.8 (1)	94.69 (5)	94.52 (8)	94.12 (9)	94.6 (1)
O11—*M*1—O21	99.5 (1)	99.62 (5)	99.70 (8)	99.40 (8)	99.5 (1)
O11—*M*1—O28	109.3 (1)	108.16 (5)	108.03 (8)	107.53 (8)	107.36 (9)
O21—*M*1—O28	113.3 (1)	111.82 (5)	111.92 (8)	112.30 (9)	112.2 (1)
O11—*M*2—O11′	180.0	180.0	180.0	180.0	180.0
O11—*M*2—O22	90.29 (9)	89.86 (5)	89.79 (7)	89.83 (8)	89.84 (9)
O11—*M*2—O22′	89.71 (9)	90.14 (5)	90.21 (7)	90.17 (8)	90.16 (9)
O11—*M*2—O29	91.72 (9)	90.68 (5)	90.68 (7)	90.82 (7)	90.97 (9)
O11—*M*2—O29′	88.28 (9)	89.32 (5)	89.32 (7)	89.18 (7)	89.03 (9)
O22—*M*2—O22′	180.0	180.0	180.0	180.0	180.0
O22—*M*2—O29	86.29 (9)	86.11 (5)	86.18 (7)	85.99 (8)	86.16 (9)
O22—*M*2—O29′	93.71 (9)	93.89 (5)	93.82 (7)	94.01 (8)	93.84 (9)
O29—*M*2—O29′	180.0	180.0	180.0	180.0	180.0

synthesis of Chen *et al.* (2003) resulted in Zn atoms interconnected by the mixed carboxylate linkers, benzene-1,4-dicarboxylic acid (H_2BDC) and benzene-1,3,5-tricarboxylic acid (H_3BTC), and DMF. The formation of the $NH_2(CH_3)_2^+$ cation could therefore relate to the synthesis conditions. However, under similar solvothermal conditions Edgar *et al.* (2001) and Clausen *et al.* (2005) obtained MOF structures based on Zn atoms, DMF solvent molecules and BDC linkers without solvent cations.

3.2. The subunits

For both (1) and (2) the bond angles and bond lengths of the benzene rings of the *BDCI*, *BDCII* and *BDCIII* linkers are very similar and close to ideal values (see supporting information[1]). The bond lengths to the carboxylate C atoms are approximately 1.5 Å. However, the torsion angles and structural surroundings of the different carboxylate groups have considerable variation. The carboxylate groups of the *BDCI* linker, O21/C21/O22 and O28/C28/O29, stabilize the metal atom subchain in the *B* layer by delocalized OCO^- groups bridging two neighboring metal atoms. The differences in C—O bond lengths are only 0.01–0.02 Å, but the carboxylate group is not completely planar with respect to the benzene ring. The O28/C28/O29 carboxylate group of (1) is twisted 18.2° for O29/C28 and 17.1° for O28/C28 with respect to the benzene ring at 120 K (Table 2). For (2) the same twists are 17.8 and 17.2° at 100 K. The O21/C21/O22 carboxylate group is only twisted 3.0° for O21/C21 and 5.4° for O22/C21 in (1) at 120 K, whereas the corresponding values are 4.1 and 5.0° for (2) at 100 K. In contrast, the *BDCII* linker, which stabilizes the void by the diagonal *top-to-bottom* bonding, is almost planar and only the terminal O12 atom is slightly twisted with respect to the benzene plane [3.2° in (1) at 120 K and 3.6° in (2) at 100 K]. The slight non-planarity of the O11/C11/O12 group with respect to the benzene ring probably originates from the hydrogen bond to O12 (H51*B*···O12 = 2.03 Å). The bond lengths of the O11/C11/O12 carboxylate group show slight localization of charge as the difference between the C—O bond lengths is ∼0.06 Å (Table 3). Thus, the negative charge of the carboxylate group is slightly more localized on O11 than on O12. The *BDCIII* linker, which bridges the *B* layers, also has one O atom (O1) bonded to the framework, and one terminal O atom (O2). The O1/C1/O2 carboxylate group also shows slight localization of charge with a C—O bond length difference of 0.06 Å (Table 3). With respect to the benzene ring the O1/C1/O2 carboxylate group twists 4.4° for O1/C1 and 5.3° for O2/C1 in (1) at 120 K. The corresponding numbers are 4.7 and 6.3° in (2) at 100 K.

The coordination of atom *M*1 (*M* = Zn and Co) is distorted tetrahedral, while the *M*2-atom coordination is tetragonally distorted octahedral (Tables 3 and 4). In the distorted *M*2 octahedron the O11 atom forms the axial bond (∼2.22 Å), whereas atoms O22 and O29 form the basal plane (∼2.04 Å). For both *M*1 and M2 there are only subtle differences in bond lengths and bond angles between (1) and (2) even though the metals are different (Tables 3 and 4). The average Co—O bond is roughly 0.01–0.03 Å longer than the corresponding Zn—O bond, except for the bridging O11 bond, which is slightly shorter for Co. For (2) the metal–ligand bond lengths and bond angles are virtually constant with temperature (Tables 3 and 4). Again the exception is the Zn2—O11 bond, which decreases in length with decreasing temperature. From 300 to 30 K this bond length changes from 2.277 (2) to 2.220 (1) Å (Table 3). However, the corresponding Co2—O11 bond in (1) is even shorter at 120 K [2.217 (2) Å]. In other words, even though the trend is that the Co—O bond lengths are longer than the corresponding Zn—O bond lengths, the axial Co2—O11 bond behaves oppositely. The unusual strength of the Co2—O11 bond correlates with the presumed magnetic interactions (see below). A carboxylate group formally has a charge of −1 e, and since there is not a strong localization of electrons in any of the carboxylate groups, each O atom formally has a net charge of −0.5 e. The two negatively charged terminal O atoms, O2 and O22, make the entire framework anionic with a net charge of −1 e. Atoms O22 and O29 both have formal charges of −0.5 e, whereas the bridging

[1] Supplementary data for this paper are available from the IUCr electronic archives (Reference: LC5040). Services for accessing these data are described at the back of the journal.

Table 5
Selected O—H bond lengths.

The last column gives the populations of the disordered C32/C33 ethyl group of *DEFI*.

	O12···H51*B*	O31···H51*A*	O2···H35*A*	O71···H55*A*	O71···H33*A*	Frac. C33*A*/C33*B*
(1): 120 K	2.04	1.86	2.54	2.58	2.40	0.57/0.43
(2): 30 K	2.03	1.86	2.52	2.55	2.32	0.57/0.43
(2): 100 K	2.03	1.86	2.52	2.55	2.39	0.56/0.44
(2): 200 K	2.05	1.86	2.53	2.45	2.86	0.91/0.09
(2): 300 K	2.08	1.86	2.49	2.43	3.04	0.92/0.08

O11 atom shares its −1/2 e charge between *M*1 and *M*2. A formal electron count suggests a +1.75 e *M*1 cation and a +2.5 e *M*2 cation, which corresponds to a mixed-valence structure. However, one may count the charges differently. O12 is a terminal framework atom bonded directly to the DEA^+ cation *via* hydrogen bonding to the positive H51*B* atom. It could therefore be argued that the formal charge of the O11/C11/O12 carboxylate group is located on atom O12, leaving O11 neutral. Since the other terminal O atom, O2, does not bond to any positively charged H atoms (O2—H35*A* $\simeq$ 2.5 Å), it can also be argued that the −1 e charge of the O1/C1/O2 group instead is located on the O1 atom. This leads to a formal electron count of +2 e for *M*1 and +2 e for *M*2, which is in better agreement with the M^{2+} sources used in the synthesis. The specific charge distribution on the framework is important for the electrostatic potential in the voids and thus for the inclusion behavior of guest species (Poulsen *et al.*, 2005). A detailed X-ray charge-density study could provide such information.

3.3. The solvent

There are two unique DEF molecules ($C_5H_{11}NO$), *DEFI* and *DEFII*, and one unique *DEA* cation ($C_4H_{12}N^+$) in the structure. Previously we have reported on MOF structures having direct bonding between the metal ions and the solvent molecules (Poulsen *et al.*, 2005). In these structures the solvent disorder was much reduced, and this allowed detailed X-ray charge-density analyses to be carried out. Although direct bonding between the solvent molecules and the framework is not observed in (1) and (2), the anisotropic thermal motion and the structural disorder of the solvent molecules can be refined on all solvent sites in (1) and (2) at temperatures below 200 K. However, for the 200 and 300 K structures of (2), large poorly shaped ellipsoids are obtained for the central N71 and C71 atoms of *DEFII*, which also lead to overall poorer convergence compared with the 30 and 100 K refinements. The problems arise from the fact that the *DEFII* molecule at these temperatures is disordered over at least two, and possibly more, positions. The charge stabilization of the anionic framework is *via* hydrogen bonding between the *DEA* cation and the negatively charged terminal O12 atom. Even though *DEA* only bonds to the framework *via* hydrogen bonding (O12···H51*B*), a series of internal hydrogen bonds amongst the solvent molecules, and from DEF to the terminal O2 atom, arrange and stabilize the positions of the three solvent sites (Table 5 and Fig. 3).

The formation of the *DEA* cation can be explained by acid-catalyzed hydrolysis (nucleophilic acylic substitution) of the DEF solvent molecule in the heated acidic solution by means of water molecules from the $M(NO_3)_2{\cdot}6H_2O$ reagent (Fig. 4). The formic acid that is formed in this reaction is not present in the crystal structure. As the carboxylate groups of the BDC linkers all bond to metal atoms, there is no obvious reason why the formate ion, $HCOO^-$, is not in the crystal. Hence, it is reasonable to assume that neither formic acid nor its derivatives are present in the reaction mixture. This can be

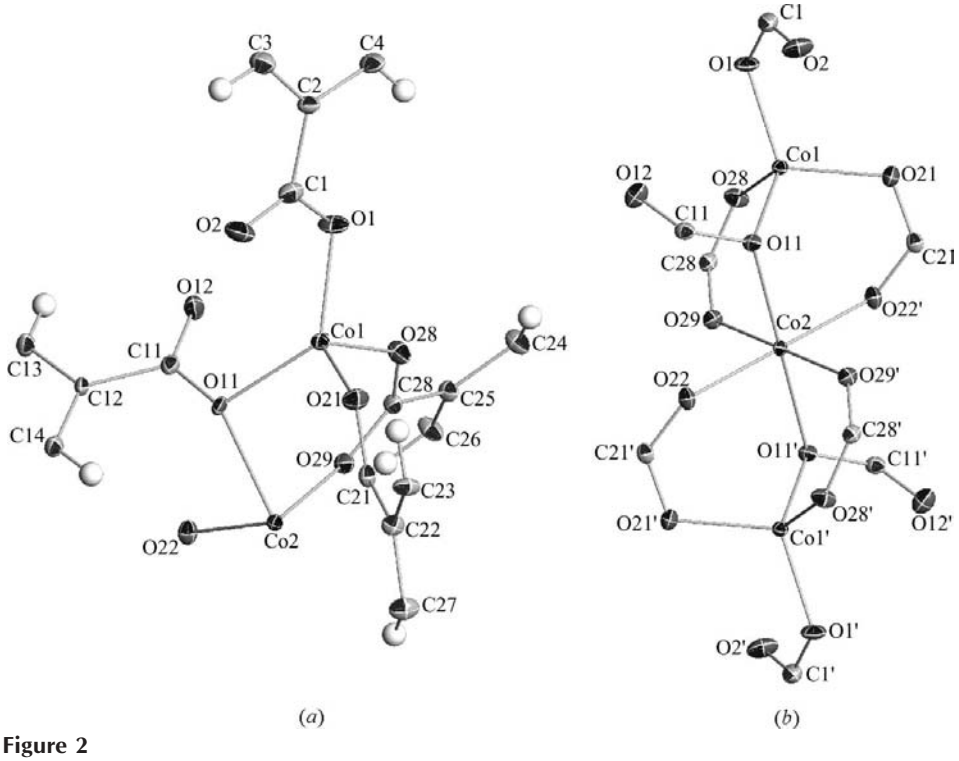

Figure 2
(*a*) The asymmetric unit of the framework for (1). (*b*) The metal atom subchain of (1), shown with the bridging carboxylate groups and the bridging O11 atom. The terminal O2 and O12 atoms are clearly visible. Compound (2) is isostructural with (1). Displacement ellipsoids are shown at the 50% level.

explained by a thermal decomposition of formic acid in the harsh environment of the autoclave. Potential decomposition reactions are $2HCOO^- \rightarrow CO + CO_2 + H_2O$, $HCOOH \rightarrow CO + H_2O$ or $HCOOH \rightarrow CO_2 + H_2$. The mechanism of the decomposition of formic acid has been studied persistently both theoretically and experimentally (Wang *et al.*, 2000; Saito *et al.*, 1984; Goddard *et al.*, 1992), but we have not found examples of synthesis conditions close to those of the present study.

From the multi-temperature structural description of the solvents in (2), it is clear that a subtle reorganization of the more isolated *DEFII* solvent molecule takes place as the temperature is lowered (Table 5). As the *DEFII* molecule moves towards the *DEFI* molecule, the O71 atom establishes a stronger hydrogen bond with the H33*A* atom, resulting in an increasingly disordered C32/C33 ethyl group (Fig. 3). From the refined populations of the disordered ethyl group it is observed that the occupancy of the minor component increases from 8% at room temperature to 43% at 30 K. In addition, the O71···H55*A* bond is shifted by +0.12 Å. Large rearrangements of the *DEA* cation and the *DEFI* molecule are not observed, because these entities are more strongly hydrogen bonded to the framework (O12···H51*B* and O31···H51*A*; see Table 5). The reorganization of the solvent is probably a result of the contraction of the unit-cell parameters as Δa(300–30 K) = 0.30, Δb(300–30 K) = 0.09, Δc(300–30 K) = −0.03 Å, $\Delta\beta$(300–30 K) = −0.26° and ΔV(300–30 K) = 102 Å^3. The large contraction of the *a* axis, along the chains, has a direct influence on the volume of the cavity in the *A* layer.

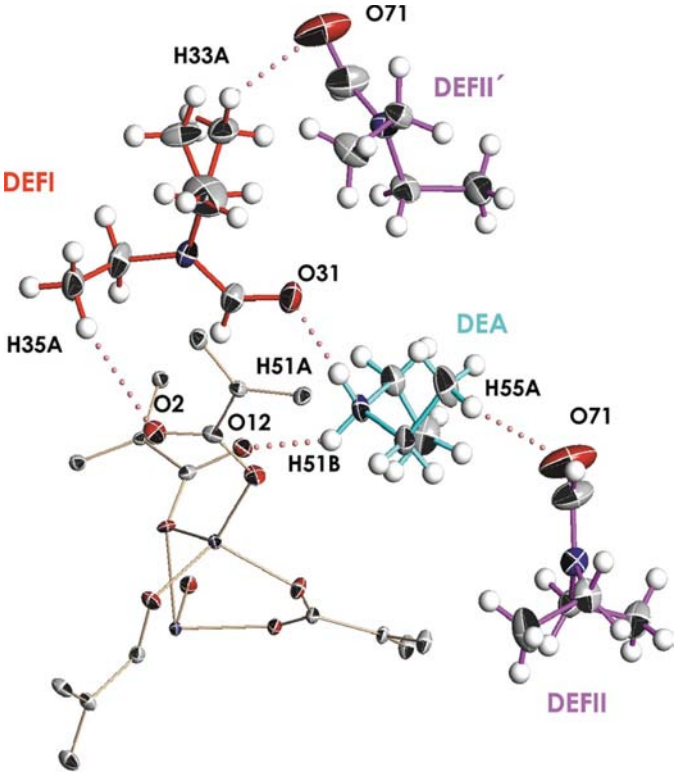

Figure 3
The asymmetric unit of (1), showing the internal solvent hydrogen bonds. The disordered C32/C33 ethyl group of the *DEFI* molecule is clearly visible, with the C33*A*/H33*A* group hydrogen bonding to the O71 atom. Displacement ellipsoids are shown at the 50% level.

3.4. Physical properties

The thermal stabilities of both compounds were examined by simultaneous TGA and DTA (Fig. 5). Even though the two compounds have the same bond connectivity the thermal decomposition schemes are quite different. Compound (1) is thermally inert up to ∼420 K, where the observed mass loss of 9% could correspond to the two DEA cations. Further mass losses of 5 and 14% at ∼520 and ∼570 K may correspond to the three DEF molecules. However, this decomposition pattern does not corroborate with the fact that the DEA cation is the stabilizer of the anionic framework, and a more complex decomposition of the solvent may occur. A complete decomposition of the framework starts at ∼720 K, where a mass loss of 33% probably corresponds to three BDC units, and ends at ∼820 K with a mass loss of 10% from the remaining BDC molecule. The heat-treated powder (after TGA/DTA) consists primarily of CoO. Compound (2) is thermally stable up to ∼370 K, where a mass loss of 8% is observed, which may correspond to one DEF molecule. A further mass loss of 25% at ∼470 K could be the remaining two DEF solvent molecules and two DEA solvent cations. The decomposition of the framework sets in at ∼570 K,

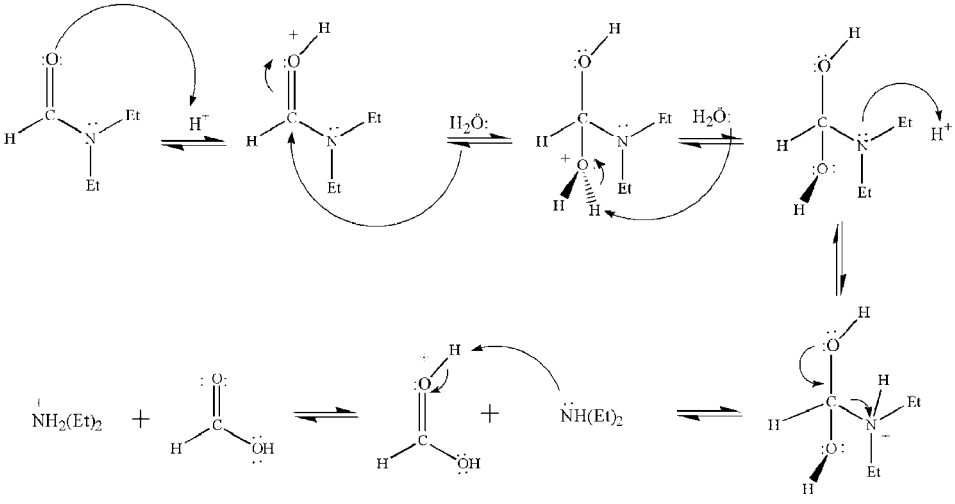

Figure 4
The acid-catalyzed hydrolysis of the DEF molecule (Lowry & Richardson, 1987).

where a mass loss of 10% equals one BDC unit, and ends at ~720 K with a mass loss of 26% corresponding to the remaining three BDC molecules. The heat-treated powder product consists of ZnO. TGA and DTA reveal that the solvent and the framework bonding energies are quite different in the two compounds. As expected both compounds initially lose the solvent molecules situated in the voids, although at different temperatures. The expulsion of the solvent in (1) starts almost 50 K above that of (2). This fact shows that the solvent molecules of (1) interact more strongly with the framework than those of (2). The decompositions of the two frameworks are also quite different. For the framework of (1), the breakdown initiates at a temperature that is 150 K above that of (2). Furthermore, it appears to completely break apart during the first decomposition step at 720 K. In contrast, the first decomposition step of (2) might originate from an initial breakdown of the layered *ABAB* crystal structure into *B* layers. Thus, the bonding of the linker to the metal centers must be different in the two frameworks.

Fig. 6 shows the magnetic susceptibility (χ) of (1) measured between 2 and 350 K. In other MOF studies we have observed that multiple crystal phases can be present in solvothermal synthesis products (Clausen *et al.*, 2005), and this will compromise measurements of bulk physical properties. However, comparisons between measured powder diffraction data and the simulated patterns of (1) and (2) show that the synthesis products are phase pure (see supporting information). The anomaly in χ at 50 K could be an onset of magnetic ordering, but the specific heat does not contain anomalies around this temperature and it may not be a bulk effect. A fit of the data above 60 K to a Curie–Weiss law [$\chi = C/(T - \Theta) + \chi_0$, where $C = N\mu_0\mu_B^2\mu_{eff}^2/(3k_B)$, N is density of magnetic ions in the relevant units, μ_{eff} is the effective moment, Θ is the Weiss temperature and χ_0 is a temperature-independent term] gives Θ = 23 K and an effective moment of 4.2 μ_B. The theoretical value of the effective moment is 3.87 μ_B for a free Co^{2+} ion with no orbital contribution and 6.54 μ_B for full orbital contribution (Ashcroft & Mermin, 1976). The magnetic susceptibility is a macroscopic property, which does not reveal the detailed atomic origin of the magnetism in the structure. No distinction is made between the two structurally distinct Co sites, nor is there consideration of covalency in the bonding, which can limit the validity of a model with magnetism centered only on the Co sites. Indeed for the antiferromagnetic MOF structure $Mn_3(C_8O_4H_4)_3(C_5H_{11}ON)_2$, the 3*d* orbital populations determined from X-ray diffraction data showed that a simple ionic picture was inadequate to explain the magnetic properties (Poulsen *et al.*, 2005). Nevertheless, if one assumes that the magnetism originates from Co ions the μ_{eff} value of 4.2 μ_B suggests substantial orbital quenching. The inset of Fig. 6 shows that the magnetization per Co atom measured at 2 K increases rapidly with magnetic field up to approximately 2 T, followed by almost complete saturation at 3 μ_B at 9 T. This field dependence is typical for ferromagnetically ordered moments, although the full saturation moment (μ_{sat}) is usually reached at lower magnetic fields. If no orbital contribution is taken into account

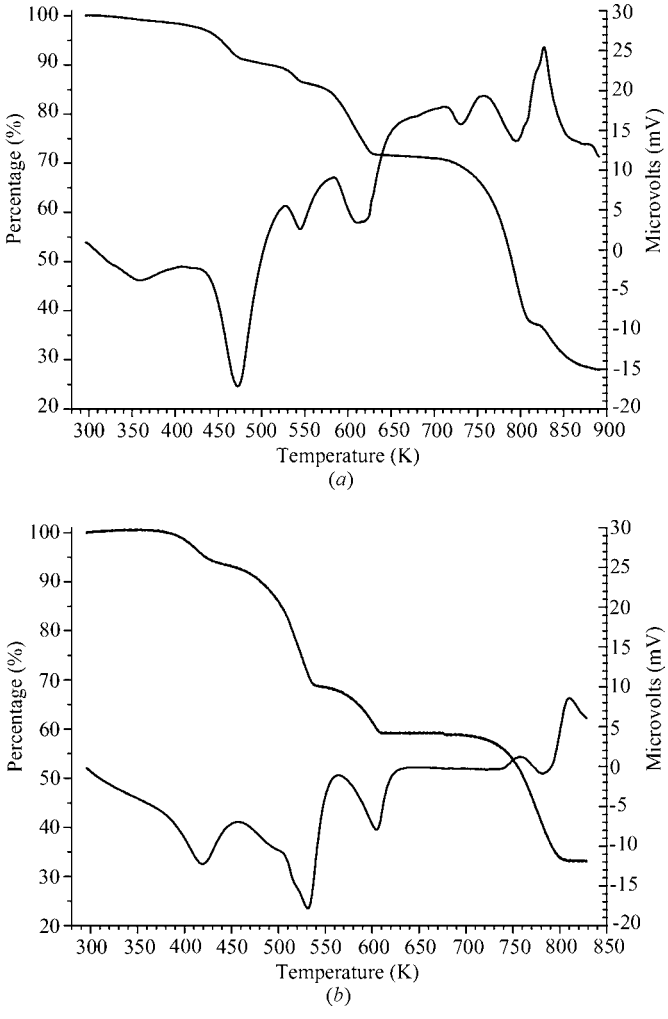

Figure 5
Thermal analysis data, TGA and DTA, for (*a*) (1) and (*b*) (2).

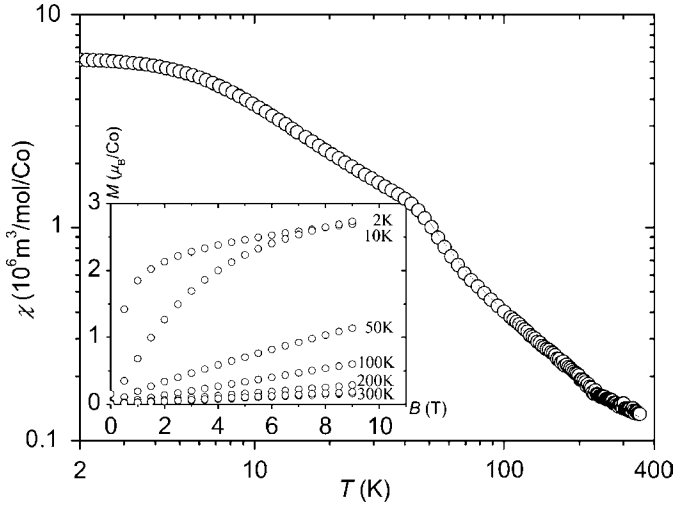

Figure 6
Magnetic susceptibility (χ) as a function of temperature (T) measured in a magnetic field (B) of 2.5 T. The black solid line is a Curie–Weiss fit of $\chi(T)$ above 50 K. The lower-left inset shows the magnetization (M) as function of B at different temperatures.

$\mu_{sat}(Co^{2+}) = 3\ \mu_B$ and $\mu_{sat}(Co^{3+}) = 4\ \mu_B$, and the saturation magnetization therefore suggests Co^{2+} ions, as is also expected from the synthesis. The positive Curie temperature corroborates a ferromagnetic ordering, and indeed the measured heat capacity reveals a phase transition at ~6 K. Fig. 7 shows the heat capacity (C_p) of both (1) and the non-magnetic (2) between 1.8 and 300 K. The high-temperature data do not superimpose for the two compounds, and therefore the two data sets have been scaled. This difference was to be expected on the basis of the TGA and DTA data, which show that even though (1) and (2) are isostructural the two compounds have different decomposition patterns and therefore different structural energies. If $(C_p/T)(T = 0\,K)$ is extrapolated to be equal to $(C_p/T)(T = 1.8\,K)$ and if the scaled data for (2) are subtracted from (1), an integration from 0 to 20 K gives an entropy of 12 J K^{-1} mol^{-1}. The calculated values [$\Delta S = R\ln(2J + 1)$] are 11.5 and 13.4 J K^{-1} mol^{-1} for Co^{2+} and Co^{3+}, respectively. This again suggests Co^{2+} ions. As for the framework potential, an X-ray charge-density study would be of considerable interest to establish the microscopic origin of the macroscopic physical properties (Poulsen *et al.*, 2005).

In the previously described Mn-based metal organic frameworks (Poulsen *et al.*, 2004, 2005), it was argued that the magnetic ordering was due to Mn–O–Mn super-exchange and not direct Mn–Mn orbital overlap. A similar mechanism may explain the magnetic ordering in the metal atom subchains, where two O11 atoms bridge the three Co atoms. As noted above the Co2—O11 bond, unlike the other *M*2—O bonds, is relatively stronger than the Zn—O11 bond. This discrepancy may be due to the magnetic interaction. In the nonmagnetic reference system (2), the Zn2—O11 bond contracts significantly with decreasing temperature, which results in the large contraction of the *a* axis. A similar structural contraction in (1) may indeed strengthen the magnetic exchange at low temperatures. Nevertheless, since magnetism is a three-dimensional property for the entire crystal, there must also be magnetic interactions in (1) involving the organic linkers. It is striking that the *BDCII* and *BDCIII* linkers have almost perfect alignment of the carboxylate and benzene π systems, whereas *BDCI* has a significant twist (Table 2). *BDCIII* molecules link the metal atom subchain, and this fact may allow the entire metal chain to align the spins. The cross-linking *BDCII* molecules then provide magnetic communication between the chains giving the three-dimensional ferromagnetic structure. The *p* orbital of the O11 atom perpendicular to the carboxylate plane is aligned along the Co—O11—Co chain and is presumably involved in this bonding. It is the same orbital that is aligned with the *BDCII* benzene π system, thus providing a three-dimensional link for the magnetism.

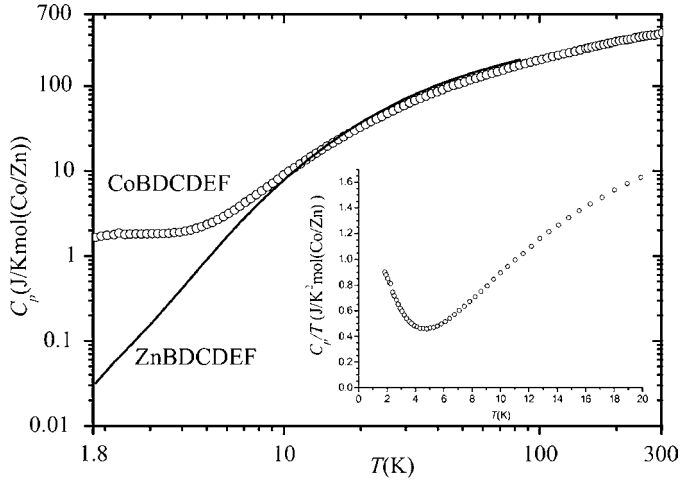

Figure 7
Specific heat (C_p) as a function of temperature (T). The inset shows the same data plotted for C_p/T as function of T

4. Conclusion

In this paper we have reported the detailed structural characterization of two new isostructural coordination polymers. The structural similarity between (1) and (2) is almost complete, and only very slight differences in bond lengths and bond angles are observed. Typically, Zn–ligand bonds are 0.01–0.03 Å shorter than the corresponding Co–ligand bonds. One notable difference is the Co2—O11 bond, which is 0.02 Å shorter than Zn2—O11. The origin of this strength is probably also the cause of the ferromagnetic ordering in the three metal atom subchains of the Co structure. The key magnetic interaction presumably is between the O11 *p* orbital perpendicular to the carboxylate plane and the Co *d* orbitals. Complete three-dimensional ordering is accomplished by alignment of the carboxylate and benzene π systems in two out of the three unique BDC linkers. The saturation magnetic moment (3 μ_B) and the effective magnetic moment (4.2 μ_B) suggest that the structure contains Co^{2+} ions. It would be of considerable interest to carry out a comparative X-ray charge density study of (1) and (2) to obtain a microscopic understanding of the macroscopic magnetic properties reported here. This has so far not been possible because of the relatively poor crystal quality of (1).

We gratefully acknowledge the beamtime obtained at beamline BM01A, the Swiss–Norwegian Beamline, ESRF, Grenoble, France. This work was supported by the DANSYNC center under the Danish Research Councils. We gratefully acknowledge Professor Judith A. K. Howard for the low-temperature diffractometer time obtained at the Department of Chemistry, University of Durham, UK, and we thank Dr Dimitrii S. Yufit and PhD student Mike R. Probert for their help during the measurement. We are indebted to the Carlsberg Foundation and the Danish Research Councils for funding a Quantum Design PPMS.

References

Ashcroft, N. W. & Mermin, N. D. (1976). *Solid State Physics.* Philidelphia: CBS Asia Publishing.

Chae, H. K., Siberio-Pérez, D. Y., Kim, J., Go, Y., Eddaoudi, M., Matzger, A. J., O'Keefe, M. & Yaghi, O. M. (2004). *Nature* (*London*), **427**, 523–527.

Chen, B. L., Eddaoudi, M., Hyde, S. T., O'Keeffe, M. & Yaghi, O. M. (2001). *Science*, **291**, 1021–1023.
Chen, W., Wang, J., Chen, C., Yue, Q., Yuan, H., Chen, J. & Wang, S. (2003). *Inorg. Chem.* **42**, 944–946.
Clausen, H. F., Poulsen, R. D., Bond, A. D., Chevalier, M. & Iversen, B. B. (2005). *J. Solid State Chem.* **178**, 3336–3345.
Eddaoudi, M., Kim, J., Rosi, N., Vodak, D., Wachter, J., O'Keeffe, M. & Yaghi, O. M. (2002). *Science*, **295**, 469–472.
Eddaoudi, M., Li, H. & Yaghi, O. M. (2000). *J. Am. Chem. Soc.* **122**, 1391–1397.
Edgar, M., Mitchell, R., Slawin, A. M. Z., Lightfoot, P. & Wright, P. A. (2001). *Chem. Eur. J.* **7**, 5168–5175.
Goddard, J. D., Yamaguchi, Y. & Schaefer, H. F. III (1992). *J. Chem. Phys.* **96**, 1158–1166.
Kitahawa, S., Kitaura, R. & Noro, S. (2004). *Angew. Chem. Int. Ed.* **43**, 2334–2375.
Kobayashi, M., Chang, H. C., Ozawa, T. C., Suzuki, M., Saktata, M. & Takata, M. (2003). *Science*, **298**, 2358–2361.
Li, H., Davis, C. E., Groy, T. L., Kelley, D. G. & Yaghi, O. M. (1998). *J. Am. Chem. Soc.* **120**, 2186–2187.
Li, H., Eddaoudi, M., O'Keeffe, M. & Yaghi, O. M. (1999). *Nature* (*London*), **402**, 276–279.
Lowry, T. H. & Richardson, K. S. (1987). *Mechanism and Theory in Organic Chemistry*, 3rd ed. New York: Harper and Row Publishers.
Lu, J. Y. (2003). *Coord. Chem. Rev.* **246**, 327–347.
Miller, J. S. & Epstein, A. J. (1995). *Chem. Eng. News*, **2**, 30–41.
Noro, S., Kitura, R., Kondo, M., Kitagawa, S., Ishii, T., Matsuzaka, H. & Yamashita, M. (2002). *J. Am. Chem. Soc.* **124**, 2568–2583.
Oxford Diffraction (2004). *CrysAlis RED*. Oxford Diffraction Ltd, Abingdon, Oxfordshire, England.
Poulsen, R. D., Bentien, A., Chevalier, M. & Iversen, B. B. (2005). *J. Am. Chem. Soc.* **127**, 9156–9166.
Poulsen, R. D., Bentien, A., Graber, T. & Iversen, B. B. (2004). *Acta Cryst.* A**60**, 382–389.
Price, D. J., Tripp, S., Powell, A. K. & Wood, P. T. (2001). *Chem. Eur. J.* **7**, 200–208.
Rosi, N., Eddaoudi, M., Kim, J., O'Keeffe, M. & Yaghi, O. M. (2002). *CrystEngComm*, **4**, 401–404.
Rosi, N., Eddaoudi, M., Vodak, D., Eckert, J., O'Keeffe, M. & Yaghi, O. M. (2003). *Science*, **300**, 1127–1129.
Rowsell, J. L. C., Spencer, E. C., Eckert, J., Howard, J. A. K. & Yaghi, O. M. (2005). *Science*, **309**, 1350–1354.
Saito, K., Kakumoto, T., Kuroda, H., Torii, S. & Imamura, A. (1984). *J. Chem. Phys.* **80**, 4989–4996.
Sheldrick, G. M. (2003). *SAINT-Plus, SADABS, XPREP* and *SHELX* programs. Bruker AXS Inc., Madison, Wisconsin, USA.
Sudik, A. C., Millward, A. R., Ockwig, N. W., Cote, A. P., Kim, J. & Yaghi, O. M. (2005). *J. Am. Chem. Soc.* **127**, 7110–7118.
Tynan, E., Jensen, P., Kelly, N. R., Kruger, P. E., Lees, A. C., Moubaraki, B. & Murray, K. S. (2004). *Dalton Trans.* pp. 3440–3447.
Yaghi, O. M., O'Keeffe, M., Ockwig, N., Chae, H. K., Eddaoudi, M. & Kim, J. (2003). *Nature* (*London*), **423**, 705–714.
Wang, B., Hou, H. & Gu, Y. (2000). *J. Phys. Chem. A*, **104**, 10526–10528.